ACS OMEGA

Open Access

http://pubs.acs.org/journal/acsodf

Article

Green Synthesis of Nickel Oxide NPs Incorporating Carbon Dots for Antimicrobial Activities

Habtamu Fekadu Etefa,* Dugasa Jabesa Nemera, and Francis Birhanu Dejene

Cite This: *ACS Omega* 2023, 8, 38418−38425

Read Online

ACCESS | Metrics & More | Article Recommendations

ABSTRACT: A biosynthesis composite using the green synthesis of titled metal nanoparticles (nickel oxide nanoparticles, NiO NPs, and carbon dots, C-dots) was produced, characterized, and then applied for antimicrobial activities. NiO NPs were produced using the *Croton macrostachyus* (*Bakkannisa*) plant leaf extract and nickel nitrate (III) hexahydrate [$Ni(NO_3)_2{\cdot}2H_2O$] as precursors, while C-dots were produced using citric acid and *o*-phenylenediamine (*o*-OPD). The distribution of the average particle size of the NiO NPs and NiO NPs@C-dots was 25.34 ± 0.12 and 24.95 ± 0.22 nm, respectively. The antimicrobial effects of the prepared materials were tested against the selected bacterial and fungal strains. Based on the outcomes of the bioassay, it was realized that both the bare and composite materials were effective against all bacterial strains. The composite's high surface area with strong inhibitive effective antimicrobial effects against bacterial and fungal strains were observed. Therefore, strong inhibitive effects of 21−24 and 22−26 mm were observed with NiO NPs and NiO NPs@C-dots, respectively.

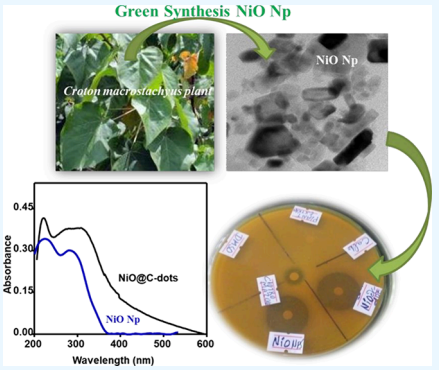

1. INTRODUCTION

Due to the size of the synthesized nanoparticle between 1 and 100 nm, at least in one dimension, nanotechnology is a rapidly developing field of science. It is an emerging technology in many areas of study, including drug treatments, cosmetics, agriculture, optics, cancer, catalysis, memory storage devices, and sensors.[1−3] Nanotechnology is an important study area in the medicine field. In medicine fields, nanoparticles can be used for cancer treatments, drug delivery, and magnetic resonance imaging.[4,5] Metal oxide nanoparticles have currently attracted many researchers. Especially, in the application of antimicrobial and antimalarial activities, other medicines, and cancer treatments, nanosized materials have special properties such as optical, magnetic, catalytic, and electrical properties as compared with bulk size materials. If the size of the compounds decreased to that of nanoparticle, it increases the surface area-to-volume ratio of the materials that can alter the physicochemical properties of nanoparticles.[6,7]

Metal oxide is one of the important transition-metal oxide nanomaterial that attracted many researchers due to its numerous applications.[8−10] NiO NPs are applicable in various areas of research including antibacterial activities, battery electrodes, photograph-electron devices, ion storage substances, gasoline sensors, magnetic substances, thermoelectric materials, gasoline cells, dye-sensitized photocathodes, electrochromic films, and cytotoxic pastime.[11,12] Various synthetic methods were used for the preparation of metal oxide nanoparticles including coprecipitation, sol−gel reaction, microemulsion, hydrothermal reaction, electrospray synthesis, and laser ablation.[13−17] However, these methods can take part in environmental pollution because of some chemicals they may release.[18] Nanoparticles synthesized by chemical and physical methods can produce nonbiodegradable materials and toxic chemicals that contribute to environmental toxicity.[19] To solve these problems, researchers have developed green and ecofriendly synthetic approaches.[20−22] Value-effective, renewable, and green organic assets may be used to prepare metal oxide nanoparticle. Synthesis of nanoparticles using plant extracts is common in the green synthesis method. These plant extracts are rich in phytochemical compounds which are effective stabilizing, capping, and reducing agents and could control the NP size and form biogenic nanoparticles.[23−25]

In this work, *Croton macrostachyus* leaf extract was used for the preparation of the titled metal oxide nanoparticle. *Croton macrostachyus* is called rush foil in English, *Bakkaniisa* in Afan Oromo, and *Bisana* in Amharic. Literature reported that the genus croton is rich in terpenoids, alkaloids, flavonoids, lignoids, proanthocyanidins, saponins, cardiac glycosides, and tannin compounds.[26−30] The fruits, leaves, and roots of *Croton macrostachyus* are used as medicine in various human and

Received: July 19, 2023
Accepted: August 24, 2023
Published: October 4, 2023

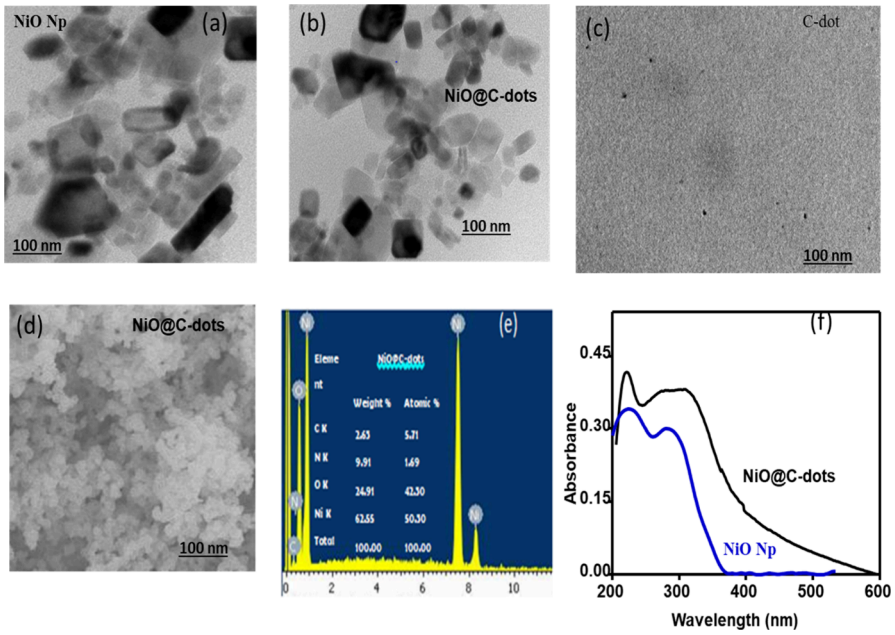

Figure 1. TEM photos of (a) NiO NPs, (b) NiO NPs@C-dots, and (c) C-dots. (d) NiO NPs@C-dots photo from the FE-SEM (e) spectra from EDS and (f) NiO NP and NiO NPs@C-dot absorption spectra in the UV−visible range.

animal diseases. Traditionally, this plant is used for the remedy of diverse sickness such as malaria, gonorrhea, rabies, diarrhea, abdominal pain, typhoid, pneumonia, and gastrointestinal disorders.[29−32]

The chemical materials of carbon compounds having the size smaller than 10 nm are known as carbon dots (C-dots).[33−36] These materials have special properties including chemiluminescence, photoluminescence, photoinduced electron transfer, and electrochemical luminescence.[33,37] C-dots find potential applications in bioimaging,[38,39] biosensing,[40,41] chemical sensing,[42] and biomedicine.[43] C-dots are the nanomaterials considered as potential candidates in the application of bioimaging, both in vitro and in vivo, and for diagnosis purposes, due to their unique fluorescent nature and having excellent biocompatibility, less cytotoxicity, and better solubility in water.[44−48] In this work, C-dots were synthesized from citric acid (CA) and *o*-phenylenediamine (*o*-OPD). The synthesized C-dots and presynthesized nickel oxide nanoparticles were used as precursors for the synthesis of nickel oxide composites of C-dot nanomaterials. The addition of C-dots on this metal oxide nanoparticle increased the antimicrobial activities.

2. EXPERIMENTAL SECTION

2.1. Reagents. Fresh and healthy leaves of *Croton macrostachyus* were collected from Jimma University. Nickel nitrate(III) hexahydrate [$Ni(NO_3)_2{\cdot}2H_2O$, 98.7%], *o*-phenylenediamine (*o*-OPD,99%), citric acid (CA, 99.5%), and ethanol (99.5%) were purchased from the market.

2.2. Synthesis of Materials. The *Croton macrostachyus* leaf extract was prepared by using the earlier reported method. To cast off undesirable ions or impurities, freshly collected plant leaves were cleaned with double distilled water and cut into fine pieces to dry easily in the open air. Using a pestle and mortar, the dried leaves were milled into fine pieces. To collect the extract compounds, 10 g of finely chopped plant leaves was weighed and dissolved in 100 mL of double distilled water. Then, the resultant solution was boiled by using a magnetic stirrer at 60 °C for 50 min. Finally, the obtained extract was cooled, filtered using a filter paper, and used for further experiments.

To synthesize nickel oxide nanoparticles, 5 g of nickel nitrate hexahydrate metal salt [$Ni(NO_3)_2{\cdot}6H_2O$] was dissolved in 40 mL of double distilled water and heated using a magnetic stirrer for 10 min. Then, in the resultant solution, 30 mL of selected leaf extract was added and constantly stirred for 4 h under ambient conditions. Following this procedure, to collect the pure compounds, the hot stirred mixture was cooled and centrifuged at 4000 rpm with ethanol, and using a furnace, it was calcined for 4 h at 450° °C. Finally, for the synthesis of the nanocomposite and characterizations, the synthesized nanoparticles were carefully placed in the sample holder. In this work, C-dots were prepared from *o*-phenylenediamine (*o*-OPD) and citric acid, according to the reported method and procedure.[49] The nanocomposites of the titled compounds were also synthesized according to the existing method and procedure.[50]

2.3. Antimicrobial Test. *2.3.1. Antibacterial Activities.* To evaluate the antibacterial activity, the method named as agar well diffusion was used against selected bacterial strains, namely, *Escherichia coli* and *Pseudomonas aeruginosa* (Gram-negative) and *Bacillus subtilis* and *Staphylococcus aureus* (Gram-positive). The method named as the McFarland standard was used to culture the bacterial strains. Following this method, bacterial cultures were activated in nutrient media and placed in an incubator at 37 °C for 24 h. Then, the bacterial strains were distributed on media plates using appropriate materials. The discs, 6 mm in diameter, were sterilized and placed into the solution of synthesized nanoparticles, nanocomposites, plant extracts, and controls. Further, the discs that contain compounds were placed onto the medium plates that had been spread with selected bacterial strains. After loading the synthesized compounds and controls on media plates, the media plates were put in an incubator at 37 °C/24 h, and the diameters of the growth inhibition zones were recorded in millimeters.[50,51]

https://doi.org/10.1021/acsomega.3c05204
ACS Omega 2023, 8, 38418−38425

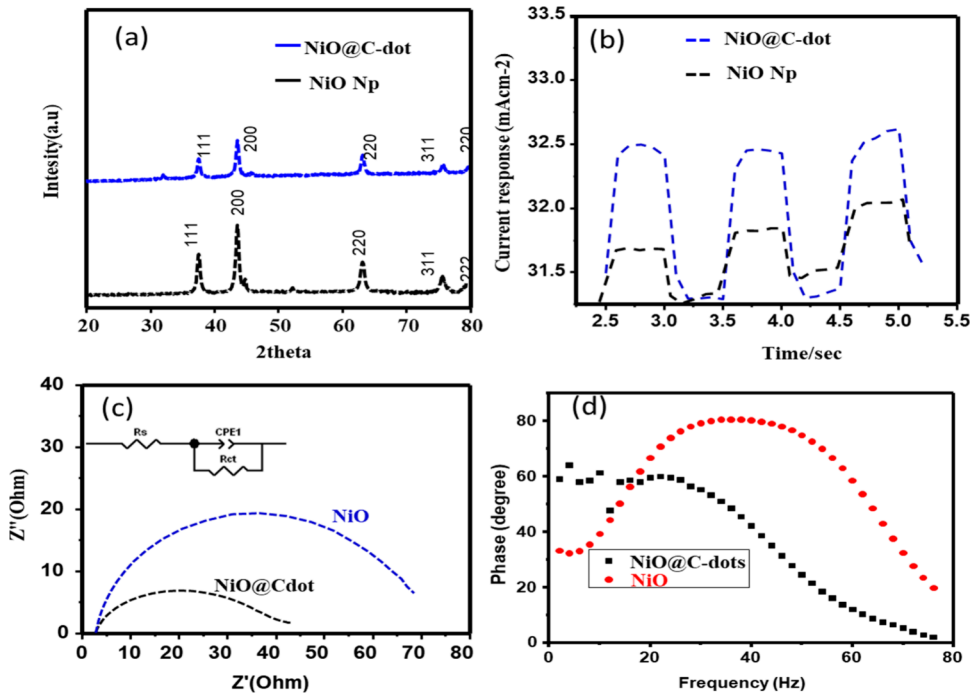

Figure 2. (a) XRD pattern of NiO NPs and NiO NPs@C-dots. (b) Transient photocurrent responses of NiO NPs and NiO NPs@C-dots. (c) Nyquist plots of EIS of NiO NPs and NiO NPs@C-dots. (d) Bode phase plots of EIS of NiO NPs and NiO NPs@C-dots.

2.3.2. Antifungul Activity. To study the antifungal activity of the synthesized materials, a method known as disc diffusion method (DDM) was used against one selected fungus, namely fuzariam. Like bacterial strains, fungul strains were also cultured and put in a shaking incubator (37 °C/24 h). To achieve antifungus activity, the media were well facilitated. Further, the cultured fungus was spread on a Petri plate, and filter paper discs of 6 mm diameter were loaded in the synthesized materials and kept on media plates. To evaluate the antifungus potential of the synthesized materials, clotrimazole and dimethyl sulfoxide were used as positive and negative controls, respectively. Finally, the media plates were placed in an incubator for 24 h/37 °C, and the zones of inhibition were recorded in millimeters.

3. RESULTS AND DISCUSSION

3.1. Material Characterization. TEM was used to evaluate the sizes and shapes of NiO NPs that were synthesized biologically (green synthesis). The rectangular NiO NP crystals (Figure 1) were found to be exactly the same as the previously reported structure. In both the TEM pictures of NiO NPs and NiO NPs/C-dots seen in Figure 1a,b, although NiO NPs and NiO NPs@C-dots have a similar shape and size (25.34 ± 0.12 and 24.95 ± 0.22 nm, respectively), C-dots cannot be visible clearly on the NiO NPs as well as in the specimens because C-dots have a lower X-ray density than NiO NPs, Thus, these findings suggest the unproven presence of C-dots in the TEM image.[52,53] However, particle size of C-dots of 2.6 nm has been found using HR-TEM of C-dots, which is a very small size (Figure 2c). FE-SEM morphology of NiO NPs@C-dots indicated a high surface area that is convenient for the antimicrobial activity. Carbon (C):nitrogen (N), C:N, ratio in the NiO NPs@C-dot composite is 1:4 at a 1.5:1 ratio of o-OPD:CA (see in Figure 1d.

As a result, with an *o*-OPD:CA mole ratio of C-dots, it was revealed that when the *o*-OPD content with the *o*-OPD:CA mixture increased (seen in Figure 1e), the concentration of oxygen lowered. Alternatively, as the *o*-OPD content inside the *o*-OPD:CA mixture increased, carbon would still have enhanced as well; however, oxygen remained constant. The UV−vis absorption spectra of NiO NPs and NiO NPs@C-dots in aqueous dispersions are shown in Figure 1f. The electronic transition from the valence band to the conductive band is responsible for the appearance of the NiO NP absorption bands at 230 and 300 nm. It is well known that the C-dot absorption bands that emerge at wavelengths of 250 and 360 nm correspond to the electron transition modes of $\pi-\pi^*$ and $n-\pi^*$, respectively.[52] The absorption bands of the NiO NPs@C-dots were identified at 345 and 230 nm; however, the 345 nm band was somewhat from the $n-\pi^*$ band of the C-dots.

The XRD peaks and peak positions, which can be seen in Figure 2a, are comparatively in good agreement with the earlier published cubic crystalline phase of NiO NPs. All index peaks appeared as (222), (311), (220), (200), and (111), from broad to sharp peaks with the lattice constants a = 4.163 and c = 2.924, which are the same with the reported constant of = 4.175.[50] Furthermore, the XRD peaks of NiO NPs@C-dots were very good with those of NiO NPs, and new peaks did not appear since the addition of C-dots had no effect on the crystal structure/crystallography of NiO NPs.

Figure 2b depicts the photocurrent response measurement of two substrates. To begin, the NiO NP and NiO NPs@C-dot film photocurrent responses were investigated to provide additional evidence on its response mechanism/behavior. The NiO NPs@C-dot film demonstrated a higher behavior of semiconductor than the NiO NP film, demonstrating the semiconductor's good photoconductive behavior. This implied that the carboxyl functional group of C-dots influenced the surface and electronic properties of NiO NPs, increasing their electrical and optical properties. The Nyquist plot of NiO NPs, on the other hand, revealed a larger semicircular arc, indicating a higher charge transfer resistance, R_{ct}, as seen in Figure 2c.

https://doi.org/10.1021/acsomega.3c05204
ACS Omega 2023, 8, 38418−38425

The resistance of this electrode was determined to be R_s = 2.5 and R_{ct} = 35 before the NiO Np treatment by C-dots. However, R_s = 2.5 and R_{ct} = 21.3 after the NiO Np treatment by C-dots. As a result, the lower R_{ct} value contributed to the material's good electrical conductivity as well as the semiconductor's increased photocurrent transient behavior. As shown in Figure 2d, relaxation time (τ_e) was calculated as a peak in the Bode phase plot. From this plot, NiO NPs revealed a relaxation time of 3.11 ms, while NiO NPs@C-dots show 5.21 ms. The higher numerical values of the relaxation time is assigned as effective/efficient for antimicrobial activity with a 1.5:1 *o*-OPD:CA molar ratio.

Because the PL intensities of NiO NPs are poor, the PL measurement is available to confirm the effects of the fluorescent material (C-dots) on the nanocomposites of metal oxides (NiO NPs@C-dots).

The PL spectra characteristics of C-dots (12 wt %) on NiO NPs at 1:1.5 (CA/*o*-OPD) mole ratios are exhibited in comparison to those of C-dots in Figure 3. The strongest blue

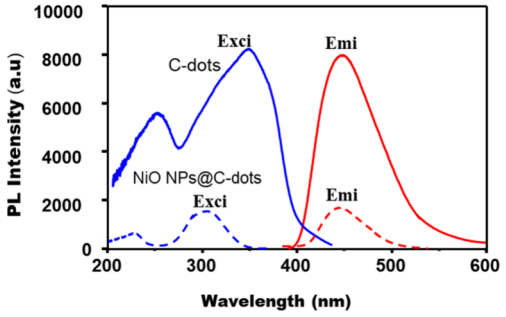

Figure 3. PL excitation (blue) and emission (red) spectra of C-dots and NiO NPs@C-dots.

emission band was seen in C-dots at 451 nm, which underwent excitation at 252 and 351 nm to provide the maximum emission intensity. It should be noted that the NiO NPs@C-dot nanocomposite materials that produced the maximum performance of antibacterial activities experienced the most quenching. The outcome suggests that NiO NPs@C-dots may have used the photon energy obtained by C-dots to increase the antimicrobial activity value.

Figure 5 shows the N2 adsorption desorption isotherms of NiO@C-dots at 12.5% C-dot contents (at a 1:1.5 CA/EDA molar ratio); the specific surface area was calculated, employing the Brunauer–Emmett–Teller (BET) technique, and the pore diameter and volume were calculated using the Barrett–Joyner–Halenda (BJH) technique.

Table 1 shows the numerical values, which can be seen in Figure 4. The isotherms were discovered to be of type IV for NiO NPs@C-dots and type III for NiO NPs. The specific surface area was the greatest at the NiO NPs@C-dots. Despite these conditions, the pore size and volume were reduced, which is similar to the situation of the maximal PCE. The

Table 1. BET Analysis of Adsorption Isotherms of NiO NPs and NiO NPs@C-Dots

materials	type	specific surface area ($m^2\ g^{-1}$)	pore size (nm)	pore volume ($cm^3\ g^{-1}$)
NiO NPs	III	22.4	17.0	0.057
NiO NPs@C-dots	IV	58.1	21.2?	0.088

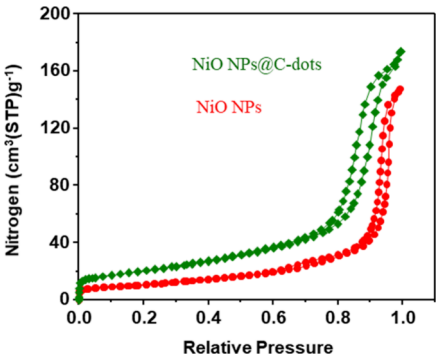

Figure 4. Nitrogen adsorption–desorption isotherms at 77 K and the analyzed parameters of NiO NPs and NiO NPs@C-dots.

enhanced surface roughness caused by the binding of C-dots is most likely what leads the composite to have more surface area when C-dots and NiO NPs coexist.

3.2. Antimicrobial Evaluation. *3.2.1. Antibacterial Evaluation.* In our study, using the method named as the agar well diffusion method, the antibacterial application of NiO NPs, its composite of carbon dots, and plant leaf extract was investigated upon *Escherichia coli*, *Bacillus cereus*, *Salmonella typhi*, and *Staphylococcus aureus* (Figure 5). In this procedure, the inhibition zone was measured in millimeters, and gentamycin and dimethyl sulfoxide were used as positive control and negative control, respectively.

The result indicates that the composite carbon dots with nickel oxide nanoparticle exhibit a significant inhibition zone (22–26 mm) compared with individual NiO NPs because the properties and the chemical composition of the bare compounds were altered. The addition of carbon dots on this metal oxide nanoparticle increased the antimicrobial activities. The effectiveness of the composites of metal oxide C-dots in killing bacteria is related to the generation of reactive oxygen species (ROS). ROS can be produced by photoexcited C-dots that can kill microorganisms (Figure 6). The inhibitory mechanism of the nanocomposites of C-dots against different bacteria and fungi includes the reaction with cellular components through various pathways including ROS generation, damage of cell wall and DNA, formation of pores in cell membranes, and cell cycle arrest, ultimately inhibiting the growth of cells. The destruction of biomolecules in cells and cell death is due to the formation of hydroxyl free radicals ($OH^{\bullet}$) and singlet oxygen ($^1O_2$) when C-dots react with the bacterial cell.

The most resistant bacteria toward NiO NPs@C-dots was *E. coli* (22 mm), but the most susceptible microorganism was *S. typhi* (26 mm). Nickel oxide nanoparticles showed the highest inhibition zone against *S. typhi* (24 mm) and smaller inhibition zone against *E. coli* (21 mm). *E. coli* may resist both bare and composite compounds in the following ways: it encodes *β*-lactamase, changes the target protein in cell wall, reduces the permeability of the outer membrane, and increases the expression of the drug efflux pump. The positive control gentamycin appeared to display an inhibition effect of 21–22 mm. The obtained inhibition data are not identical, and the result indicates the effectiveness of the compounds against the selected bacterial strain. The differences may be due to the impermeability of the bacterial cells or the variation in ribosomes that appeared in the bacterial cells. Also, the effectiveness of the synthesized compounds may be dependent

https://doi.org/10.1021/acsomega.3c05204
ACS Omega 2023, 8, 38418–38425

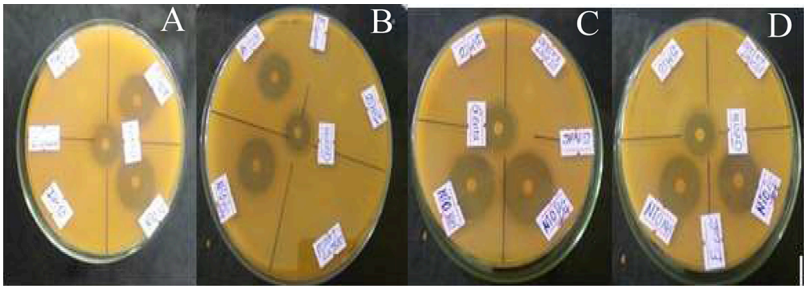

Figure 5. In vitro antibacterial activity of Croton macrostachyus leaf extract, NiO NPs, NiO NPs/C-dots, gentamycin, and DMSO against (A) *S. aureus*, (B) *B. cereus*, (C) *S. typhi*, and (D) *E. coli*.

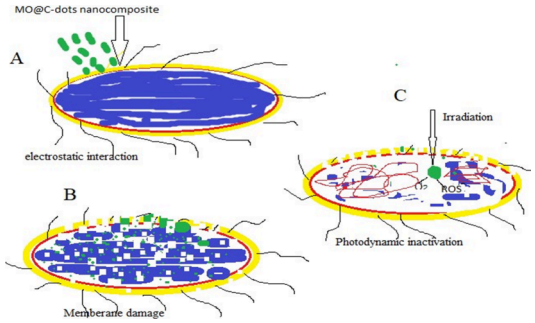

Figure 6. General bactericidal mechanisms of action of MO@C-dots. (A) Interaction of MO@C-dots with the bacterial cell wall. (B) MO@C-dot internalization, intercalation in the bacterial membrane, and irreversible disruption with a leak of cytoplasmic material. (C) MO@C-dots promoted bacterial photodynamic inactivation with ROS production and DNA damage.

on the interaction between the synthesized compounds and receptor molecules. The surface of the synthesized nanoparticles and nanocomposites carries a positive charge, while the microbial cell wall has an opposite charge. Consequently, the reaction between these charges results in the damage of the bacterial wall as well as cytoplasm. Also, the metal oxide nanoparticle can give ROS that leads to protein oxidation and DNA destruction, which damage the bacteria. Generally, the Croton macrostachyus leaf aqueous extract-treated synthesized nanocomposite exhibited more antibacterial activity compared to the other reported compounds against the selected bacterial strain.[53,54] In contrast to gentamycin, all bacterial strains were of 21−26 mm for *S. typhi* (Table 2) against the hindrance zone. This outcome, the effect of these materials on selected bacterial strains, was not uniform. Such an alternative can occur due to the stiffness of the structures' containers or differences in ribosomes that arose in the microbial containers. This discipline may also be applied to the strong reaction between compounds and receptor fragments. Furthermore, while the present work was compared with the literature, the inhibition zone of microbial activities was better than that reported in the literature. When we compared our work with the findings in recent reported papers (see Table 2), our present work showed inhibition zones. Additionally, compared to just individual NiO NPs, the presence of C-dots raised the size of the inhibition zone, which is assigned to the influence of C-dots.

3.2.2. Antifungal Evaluation. Antifungal applications of the synthesized NiO NPs, NiO NPs@C-dots, and plant leaf extract were studied against the Candida albicans fungus strain (Figure 7). Clotrimazole was used as a positive control. Our results

Table 2. Antimicrobial Activity of the Reported and Present Material Compositions

materials	synthesis method	bacteria strain	in inhibition zone (mm)	ref.
NiO NPs	biosynthesis	*E. coli*	18, 22	48
		S. aureus	15, 19	
		B. cereus	14	
		S. typhi	20	
NiO NPs@C-dots	biosynthesis	*E. coli*	23	48
		S. aureus	17	
		B. cereus	20	
		S. typhi	21	
ZnO NPs	biosynthesis	*E. coli*	18, 25.30	55−57
		S. aureus	25.30	
		B. cereus	-	
		S. typhi	-	
α-Fe_2O_3 NPs		*E. coli*	10	58
		S. aureus	-	
		B. cereus	-	
		S. typhi	-	
C. cassia (plant extract)		*E. coli*	15	59
		S. aureus	22	
		B. cereus	-	
		S. typhi	8	
NiO NPs	biosynthesis	*E. coli*	21	present work
		S. aureus	23	
		B. cereus	23	
		S. typhi	24	
NiO NPs@C-dots	biosynthesis	*E. coli*	22	present work
		S. aureus	25	
		B. cereus	23	
		S. typhi	26	

concluded that the prepared NiO NPs@C-dots showed a higher inhibition zone (24 mm) compared with NiO NPs (22 mm). The standard drug clotrimazole showed a lower inhibition zone (16 mm), and the *Croton macrostachyus* leaf aqueous extract was not active against the selected fungus strain.

4. CONCLUSIONS

In summary, a composite made of hydrothermally green-synthesized NiO nanostructures with C-dots and the prepared compounds has been tested for its antimicrobial properties in the current research. The reactive functional group of C-dots caused the composite to have increased antimicrobial activities in accordance with this. Due to the reaction between the receptor compounds (amino acid molecules) and the functional groups of C-dots, the antimicrobial (antibacterial and

https://doi.org/10.1021/acsomega.3c05204
ACS Omega 2023, 8, 38418−38425

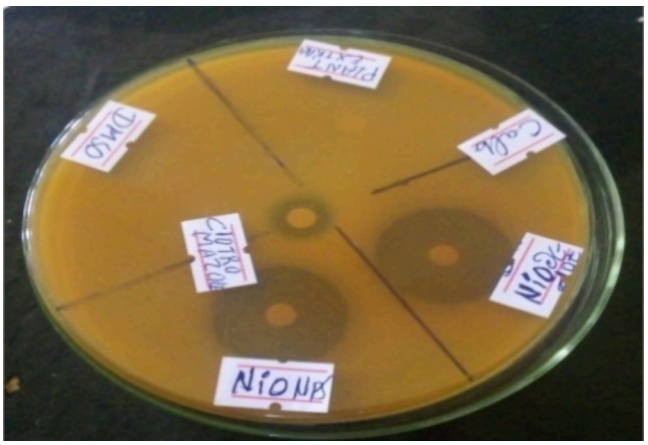

Figure 7. In vitro fungal evaluation of the Croton macrostachyus leaf extract, NiO NPs, NiO NPs/C-dots, gentamycin, and dimethyl sulfoxide against the Candida albicans fungus strain.

antifungal) activities of the synthesized nanocomposite was increased. C-dots are therefore regarded as having a less harmful effect due to their clearness and cost-effectiveness. As a result, we have seen that NiO NPs@C-dot composites are much more effective against a particular bacterial strain than their metal oxide nanoparticle counterparts.

AUTHOR INFORMATION

Corresponding Author

Habtamu Fekadu Etefa − *Department of Physics, Walter Sisulu University, Mthatha 5117, South Africa; Department of Physics, College of Natural and Computation Science, Dambi Dollo University, Dambi Dollo, Addis Ababa 260, Ethiopia;* orcid.org/0000-0002-5638-1231; Phone: +27781011307; Email: habtamufekadu24@gmail.com

Authors

Dugasa Jabesa Nemera − *Department of Chemistry, College of Natural Sciences, Jimma University, Jimma 11, Ethiopia*

Francis Birhanu Dejene − *Department of Physics, Walter Sisulu University, Mthatha 5117, South Africa*

Complete contact information is available at: https://pubs.acs.org/10.1021/acsomega.3c05204

Author Contributions

H.F.E., D.J.N., and F.B.D. contributed equally to the following tasks: inquiry, formal analysis and writing, original draft preparation, conceptualization, methodology, resources, reviewing, editing, visualization, and supply of conceptual ideas and data analysis, as well as formal analysis and writing.

Notes

The authors declare no competing financial interest.

ACKNOWLEDGMENTS

The authors express their sincere gratitude to Walter Sisulu University (WSU) and ESKOM for the financial support.

REFERENCES

(1) Abbasi, B. A.; Iqbal, J.; Nasir, J. A.; Zahra, S. A.; Shahbaz, A.; Uddin, S.; Hameed, S.; Gul, F.; Kanwal, S.; Mahmood, T. Environmentally friendly green approach for the fabrication of silver oxide nanoparticles: Characterization and diverse biomedical applications. *Microsc. Res. Techn.* **2020**, *83*, 1308−1320.

(2) Hussein, B. Y.; Mohammed, A. M. Biosynthesis and characterization of nickel oxide nanoparticles by using aqueous grape extract and evaluation of their biological applications. *Results Chem.* **2021**, *3*, No. 100142.

(3) Pokrajac, L.; Abbas, A.; Chrzanowski, W.; Dias, G.; Eggleton, B.; Maguire, S.; Maine, E.; Malloy, T. F.; Nathwani, J.; Nazar, L. Nanotechnology for a Sustainable Future: Addressing Global Challenges with the International Network4Sustainable Nanotechnology. *UCLA School of Law, Public Law Research Paper* **2022**, 15.

(4) Hao, R.; Xing, R.; Xu, Z.; Hou, Y.; Gao, S.; Sun, S. Synthesis, functionalization, and biomedical applications of multifunctional magnetic nanoparticles. *Adv. Mater.* **2010**, *22*, 2729−2742.

(5) Brigger, I.; Dubernet, C.; Couvreur, P. Nanoparticles in cancer therapy and diagnosis. *Adv. Drug Deliv. Rev.* **2012**, *64*, 24−36.

(6) Krishnan, V.; Bupesh, G.; Manikandan, E.; Thanigai, A.; Magesh, S.; Kalyanaraman, R.; Maaza, M. Green synthesis of silver nanoparticles using Piper nigrum concoction and its anticancer activity against MCF-7 and Hep-2 cell lines. *J. Antimicro* **2016**, *2*, 123.

(7) Jadoun, S.; Arif, R.; Jangid, N. K.; Meena, R. K. Green synthesis of nanoparticles using plant extracts: *A review*. *Environ. Chem. Lett.* **2021**, *19*, 355−374.

(8) Jawad, N.; Hassan, K. Structural Characterization of NiO Nanoparticles Prepared by Green Chemistry Synthesis Using Arundo donaxi Leaves Extract. In *Journal of Physics: Conference Series*; IOP Publishing, 2021; vol *1818*.

(9) Anand, G. T.; Nithiyavathi, R.; Ramesh, R.; Sundaram, S. J.; Kaviyarasu, K. Structural and optical properties of nickel oxide nanoparticles: *Investigation of antimicrobial applications*. *Surf. Interfaces* **2020**, *18*, No. 100460.

(10) Rajan, P. I.; Vijaya, J. J.; Jesudoss, S.; Kaviyarasu, K.; Kennedy, L. J.; Jothiramalingam, R.; Al-Lohedan, H. A.; Vaali-Mohammed, M.-A. Green-fuel-mediated synthesis of self-assembled NiO nano-sticks for dual applications—photocatalytic activity on Rose Bengal dye and antimicrobial action on bacterial strains. *Mater. Res. Express* **2017**, *4*, No. 085030.

(11) Ezhilarasi, A. A.; Vijaya, J. J.; Kennedy, L. J.; Kaviyarasu, K. Green mediated NiO nano-rods using Phoenix dactylifera (Dates) extract for biomedical and environmental applications. *Mater. Chem. Phys.* **2020**, *241*, No. 122419.

(12) Fardood, S. T.; Ramazani, A.; Moradi, S. A novel green synthesis of nickel oxide nanoparticles using Arabic gum. *Chem. J. Moldova* **2017**, *12*, 115−118.

(13) Imran Din, M.; Rani, A. Recent advances in the synthesis and stabilization of nickel and nickel oxide nanoparticles: a green adeptness. *Int. J. Anal. Chem.* **2016**, *2016*, No. 3512145.

(14) Petcharoen, K.; Sirivat, A. Synthesis and characterization of magnetite nanoparticles via the chemical co-precipitation method. *Mater. Sci. Eng., B* **2012**, *177*, 421−427.

(15) Jia, F.; Zhang, L.; Shang, X.; Yang, Y. Non-Aqueous Sol−Gel Approach towards the Controllable Synthesis of Nickel Nanospheres, Nanowires, and Nanoflowers. *Adv. Mater.* **2008**, *20*, 1050−1054.

(16) Basak, S.; Chen, D.-R.; Biswas, P. Electrospray of ionic precursor solutions to synthesize iron oxide nanoparticles: modified scaling law. *Chem. Eng. Sci.* **2007**, *62*, 1263−1268.

(17) Yang, G. Laser ablation in liquids: Applications in the synthesis of nanocrystals. *Prog. Mater. Sci.* **2007**, *52*, 648−698.

(18) Thema, F.; Manikandan, E.; Gurib-Fakim, A.; Maaza, M. Single phase Bunsenite NiO nanoparticles green synthesis by Agathosma betulina natural extract. *J. Alloys Compd.* **2016**, *657*, 655−661.

(19) Ismail, E.; Diallo, A.; Khenfouch, M.; Dhlamini, S.; Maaza, M. RuO2 nanoparticles by a novel green process via Aspalathus linearis natural extract & their water splitting response. *J. Alloys Compd.* **2016**, *662*, 283−289.

(20) Sudha, A.; Jeyakanthan, J.; Srinivasan, P. Green synthesis of silver nanoparticles using Lippia nodiflora aerial extract and evaluation of their antioxidant, antibacterial and cytotoxic effects. *Resource-Efficient Technol.* **2017**, *3*, 506−515.

https://doi.org/10.1021/acsomega.3c05204
ACS Omega 2023, 8, 38418−38425

(21) Abbasi, B. A.; Iqbal, J.; Khan, Z.; Ahmad, R.; Uddin, S.; Shahbaz, A.; Zahra, S. A.; Shaukat, M.; Kiran, F.; Kanwal, S. Phytofabrication of cobalt oxide nanoparticles from Rhamnus virgata leaves extract and investigation of different bioactivities. *Microsc. Res. Techn.* **2021**, *84*, 192−201.
(22) Uddin, S.; Safdar, L. B.; Anwar, S.; Iqbal, J.; Laila, S.; Abbasi, B. A.; Saif, M. S.; Ali, M.; Rehman, A.; Basit, A. Green synthesis of nickel oxide nanoparticles from Berberis balochistanica stem for investigating bioactivities. *Molecules* **2021**, *26*, 1548.
(23) Iqbal, J.; Abbasi, B. A.; Mahmood, T.; Kanwal, S.; Ali, B.; Shah, S. A.; Khalil, A. T. Plant-derived anticancer agents: A green anticancer approach. *Asian Pacific J. Trop. Biomed.* **2017**, *7*, 1129−1150.
(24) Iqbal, J.; Abbasi, B. A.; Batool, R.; Mahmood, T.; Ali, B.; Khalil, A. T.; Kanwal, S.; Shah, S. A.; Ahmad, R. Potential phytocompounds for developing breast cancer therapeutics: nature's healing touch. *Eur. J. Pharmacol.* **2018**, *827*, 125−148.
(25) Kar, A.; Ray, A. K. Synthesis of nano-spherical nickel by templating hibiscus flower petals. *J. Nanosci. Nanotechnol.* **2014**, *2*, 17−20.
(26) Carlet, J.; Jarlier, V.; Harbarth, S.; Voss, A.; Goossens, H.; Pittet, D. *BioMed. Cent.* **2012**, *1*, 1−13.
(27) Käppeli, U.; Hächler, H.; Giezendanner, N.; Beutin, L.; Stephan, R. Human infections with non-O157 Shiga toxin−producing Escherichia coli, Switzerland, 2000−2009. *Emerg. Infect. Dis.* **2011**, *17*, 180.
(28) ChB, K.; Krishnaiah, N.; Mallika, E. Escherichia coli O157: H7-An emerging pathogen in foods of animal origin. *Vet. World* **2010**, *3*, 382−389.
(29) Abdisa, T. Medicinal value of Croton macrostachyus and Solanum incanum against causative agent of foodborne diseases. *Vet. Med.* **2019**, *4*, 57−68.
(30) Bantie, L.; Assefa, S.; Teklehaimanot, T.; Engidawork, E. In vivo antimalarial activity of the crude leaf extract and solvent fractions of Croton macrostachyus Hocsht.(Euphorbiaceae) against Plasmodium berghei in mice. *BMC Complement. Altern. Med.* **2014**, *14*, 79.
(31) Krishnaiah, D.; Sarbatly, R.; Bono, A. Phytochemical antioxidants for health and medicine: A move towards nature. *Biotechnol. Mol. Biol. Rev.* **2007**, *1*, 97−104.
(32) Lee, J. H. Methicillin (oxacillin)-resistant Staphylococcus aureus strains isolated from major food animals and their potential transmission to humans. *Appl. Environ. Microbiol.* **2003**, *69*, 6489−6494.
(33) Wang, Y.; Hu, A. Carbon quantum dots: synthesis, properties and applications. *J. Mater. Chem. C* **2014**, *2*, 6921−6939.
(34) Wang, Y.; Chen, D.; Zhang, J.; Balogun, M. S.; Wang, P.; Tong, Y.; Huang, Y. Charge relays via dual carbon-actions on nanostructured BiVO4 for high performance photoelectrochemical water splitting. *Adv. Funct. Mater.* **2022**, *32*, No. 2112738.
(35) Li, Y.; Xia, Y.; Liu, K.; Ye, K.; Wang, Q.; Zhang, S.; Huang, Y.; Liu, H. Constructing Fe-MOF-derived Z-scheme photocatalysts with enhanced charge transport: nanointerface and carbon sheath synergistic effect. *ACS Appl. Mater. Interfaces* **2020**, *12*, 25494−25502.
(36) Di Mare, M.; Ouellet-Plamondon, C. *Mater. Today Sustain.* **2022**, *20*, No. 100261.
(37) Dong, Y.; Wang, R.; Li, G.; Chen, C.; Chi, Y.; Chen, G. Polyamine-functionalized carbon quantum dots as fluorescent probes for selective and sensitive detection of copper ions. *Anal. Chem.* **2012**, *84*, 6220−6224.
(38) Tao, H.; Yang, K.; Ma, Z.; Wan, J.; Zhang, Y.; Kang, Z.; Liu, Z. In vivo NIR fluorescence imaging, biodistribution, and toxicology of photoluminescent carbon dots produced from carbon nanotubes and graphite. *Small* **2012**, *8*, 281−290.
(39) Gao, X.; Cui, Y.; Levenson, R. M.; Chung, L. W.; Nie, S. In vivo cancer targeting and imaging with semiconductor quantum dots. *Nat. Biotechnol.* **2004**, *22*, 969−976.
(40) Peng, H.; Zhang, L.; Kjällman, T. H.; Soeller, C.; Travas-Sejdic, J. DNA hybridization detection with blue luminescent quantum dots and dye-labeled single-stranded DNA. *J. Am. Chem. Soc.* **2007**, *129*, 3048−3049.
(41) Zhang, Y.; Cui, P.; Zhang, F.; Feng, X.; Wang, Y.; Yang, Y.; Liu, X. Fluorescent probes for "off−on" highly sensitive detection of Hg2+ and L-cysteine based on nitrogen-doped carbon dots. *Talanta* **2016**, *152*, 288−300.
(42) Sharma, V.; Tiwari, P.; Mobin, S. M. Sustainable carbon-dots: recent advances in green carbon dots for sensing and bioimaging. *J. Mater. Chem. B* **2017**, *5*, 8904−8924.
(43) Chen, F.; Gao, W.; Qiu, X.; Zhang, H.; Liu, L.; Liao, P.; Fu, W.; Luo, Y. Graphene quantum dots in biomedical applications: recent advances and future challenges. *Front. Lab. Med.* **2017**, *1*, 192−199.
(44) Liu, C.; Zhang, P.; Zhai, X.; Tian, F.; Li, W.; Yang, J.; Liu, Y.; Wang, H.; Wang, W.; Liu, W. Nano-carrier for gene delivery and bioimaging based on carbon dots with PEI-passivation enhanced fluorescence. *Biomaterials* **2012**, *33*, 3604−3613.
(45) Etefa, H. F.; Kumar, V.; Dejene, F. B.; Efa, M. T.; Jule, L. T. Modification of Flexible Electrodes for P-Type (Nickel Oxide) Dye-Sensitized Solar Cell Performance Based on the Cellulose Nanofiber Film. *ACS Omega* **2023**, *8* (17), 15249−15258.
(46) Zheng, M.; Ruan, S.; Liu, S.; Sun, T.; Qu, D.; Zhao, H.; Xie, Z.; Gao, H.; Jing, X.; Sun, Z. Self-targeting fluorescent carbon dots for diagnosis of brain cancer cells. *ACS Nano* **2015**, *9*, 11455−11461.
(47) Sharma, A.; Das, J. Small molecules derived carbon dots: synthesis and applications in sensing, catalysis, imaging, and biomedicine. *J. Nanobiotechnol.* **2019**, *17*, 92.
(48) Nemera, D. J.; Etefa, H. F.; Kumar, V.; Dejene, F. B. Hybridization of nickel oxide nanoparticles with carbon dots and its application for antibacterial activities. *Luminescence* **2022**, *37*, 965−970.
(49) Kumar, V.; Etefa, H. F.; Efa, M. T.; Jule, L. T. Hybrid 1D Semiconducting ZnO and GaN Nanostructures for Light-Emitting Devices. *1D Semiconducting Hybrid Nanostructures: Synthesis and Applications in Gas Sensing and Optoelectronics* **2023**, 205−216.
(50) Etefa, H. F.; Imae, T.; Yanagida, M. Enhanced photosensitization by carbon dots Co-adsorbing with dye on p-type semiconductor (Nickel Oxide) solar cells. *ACS Appl. Mater. Interfaces* **2020**, *12*, 18596−18608.
(51) Gemeda, G. F.; Etefa, H. F.; Hsieh, C.-C.; Kebede, M. A.; Imae, T.; Yen, Y.-W. Preparation of ZnO/NiO-loaded flexible cellulose nanofiber film electrodes and their application to dye-sensitized solar cells. *Carbohydr. Polym. Technol. Appl.* **2022**, *3*, No. 100213.
(52) Vijaya Kumar, P.; Jafar Ahamed, A.; Karthikeyan, M. Synthesis and characterization of NiO nanoparticles by chemical as well as green routes and their comparisons with respect to cytotoxic effect and toxicity studies in microbial and MCF-7 cancer cell models. *SN Appl. Sci.* **2019**, *1*, 1083.
(53) Ezhilarasi, A. A.; Vijaya, J. J.; Kaviyarasu, K.; Kennedy, L. J.; Ramalingam, R. J.; Al-Lohedan, H. A. Green synthesis of NiO nanoparticles using Aegle marmelos leaf extract for the evaluation of in-vitro cytotoxicity, antibacterial and photocatalytic properties. *J. Photochem. Photobiol., B* **2018**, *180*, 39−50.
(54) Kumar, C. R.; Betageri, V. S.; Nagaraju, G.; Pujar, G.; Suma, B.; Latha, M. Photocatalytic, nitrite sensing and antibacterial studies of facile bio-synthesized nickel oxide nanoparticles. *J. Sci.: Adv. Mater. Devices* **2020**, *5*, 48−55.
(55) Abebe, B.; Zereffa, E. A.; Tadesse, A.; Murthy, H. A. A review on enhancing the antibacterial activity of ZnO: Mechanisms and microscopic investigation. *Nanoscale Res. Lett.* **2020**, *15*, 190.
(56) Meraat, R.; Ziabari, A. A.; Issazadeh, K.; Shadan, N.; Jalali, K. M. Synthesis and characterization of the antibacterial activity of zinc oxide nanoparticles against Salmonella typhi. *Acta Metallurgica Sinica (English Letters)* **2016**, *29*, 601−608.
(57) Prasad, A. R.; Basheer, S. M.; Gupta, I. R.; Elyas, K.; Joseph, A. Investigation on bovine serum albumin (BSA) binding efficiency and antibacterial activity of ZnO nanoparticles. *Mater. Chem. Phys.* **2020**, *240*, No. 122115.
(58) Naz, S.; Islam, M.; Tabassum, S.; Fernandes, N. F.; de Blanco, E. J. C.; Zia, M. Green synthesis of hematite (α-Fe2O3) nanoparticles using Rhus punjabensis extract and their biomedical prospect in pathogenic diseases and cancer. *J. Mol. Struct.* **2019**, *1185*, 1−7.

https://doi.org/10.1021/acsomega.3c05204
ACS Omega 2023, 8, 38418−38425

(59) Ali, S. K.; Ali, G. S.; Abdullah, B. A. In vitro antibacterial activities of various ethanolic medicinal plant extracts against some human pathogenic bacteria. *Turk. J. Agric.-Food Sci. Technol.* **2020**, *8*, 1272−1276.

https://doi.org/10.1021/acsomega.3c05204
ACS Omega 2023, 8, 38418−38425